The toxicological impact of nanoparticles

Nanotechnology is a relatively new and vast field. The increased presence of nanomaterials in commercial products such as cosmetics and sunscreens, dental fillings, photovoltaic cells, and water filtration and catalytic systems has resulted in a growing public debate on the toxicological and environmental effects of direct and indirect exposure to these materials. At present, these effects are not completely elucidated.

Roberta Brayner
Interfaces, Traitements, Organisation et Dynamique des Systèmes (ITODYS), Université Paris Diderot, UMR-CNRS 7086, case 7090, 2 place Jussieu, 75251 Paris Cedex 05, France
E-mail: roberta.brayner@univ-paris-diderot.fr

Even though nanotechnology is a fairly new field, nanomaterials are not. Au and Ag nanoparticles (NPs) were used in Persia in the 10th century BC to fabricate ceramic glazes to provide a lustrous or iridescent effect. This technique was then brought to Spain, where it was improved by the Moors during the 14th century, before finally spreading throughout much of Europe[1]. In addition, over 5000 years ago, the Egyptians ingested Au NPs for mental and bodily purification[2]. In all cases, the users did not know that they were NPs.

The study of the toxicity of nanomaterials toxicity on living cells and within the context of environmental air pollution is a very large research field[3]. Here I show some relevant studies of the toxicological impact of (i) oxide NPs (TiO_2 and ZnO), (ii) carbon-based nanomaterials, and (iii) Au NPs on living cells. Finally, at the end of this review, I discuss the toxicity of some kinds of inhaled NPs.

TiO_2 and ZnO nanoparticles

Nowadays, NPs are frequently found commercially as cosmetics and sunscreens (TiO_2, Fe_3O_4, and ZnO), fillers in dental fillings (SiO_2), in water filtration and catalytic systems, and in photovoltaic cells (CdS, CdSe, ZnS), etc. Unfortunately, toxicological studies carried out in the last ten years have shown that ultrafine particles (d <100 nm) pose serious problems to the lungs[4–6]. It has been demonstrated that some NPs cause more inflammation than larger respirable particles made from the same material when delivered at the same mass dose. This behavior has been observed for a range of different materials of generally low toxicity such as carbon black (CB) and TiO_2[7]. For example, micronized or ultrafine (20–50 nm) TiO_2, a so-called microreflector, (US Federal Register, 43FR38206, 25 August 1978) has been known to be a safe physical sunscreen because it reflects and scatters ultraviolet (UV) B and UVA in sunlight. However, TiO_2 absorbs about 70% of incident UV and in aqueous environments this leads to the generation of hydroxyl radicals. The crystalline forms of TiO_2, *anatase* and *rutile*, are semiconductors with gap energies of about 3.23 and 3.06 eV respectively[8]. Consequently, light at or below these wavelengths contains enough energy to promote electrons from the valence band (vb) to the conduction band (cb), generating single electrons (e^-) and positively charged holes (h^+) as carriers (Fig. 1).

Electrons and holes often recombine quickly, but they can also migrate to the particle surface, where they react with adsorbed species:

ISSN:1748 0132 © Elsevier Ltd 2008

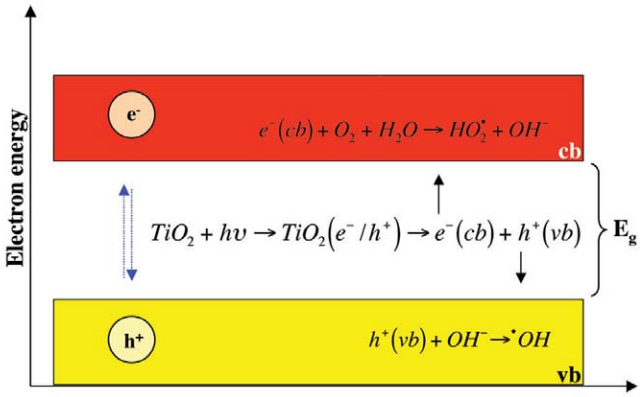

Fig. 1 Simplified semiconductor bandgap structure and schematic formation of superoxide and hydroxyl radicals.

(i) electrons react with oxygen and (ii) holes with hydroxyl ions or water to form superoxide and hydroxyl radicals (Fig. 1).

According to Dunford *et al.*[8], such photo-oxidations may explain the toxicity of illuminated TiO_2 and its possible effects on DNA. The authors studied commercial TiO_2 samples (20–50 nm in diameter) with different anatase/rutile ratios (some samples also contained ZnO) following illumination of DNA *in vivo* using comet assays. The comet assay is a single-cell based technique that allows detection and quantification of DNA damage. The assay uses nuclei embedded in agarose and exposed to an electric field. In these assays, human cells (MRC-5 fibroblasts) were illuminated on ice with or without a TiO_2-containing sunscreen. The study demonstrates that DNA in human cells is damaged by illumination in the presence of TiO_2 (Fig. 2). In addition, suppression by the quencher dimethyl sulfoxide (DMSO) implies that the damage is caused by hydroxyl radicals[8]. According to the authors, these assays detect direct strand breaks and alkali-labile sites, and reveal the damage attributable to TiO_2.

The fate of these NPs, when applied to human skin, is not completely understood. Moreover, some autoradiographic studies using ^{65}ZnO suggest that such particles can pass through rat and rabbit skin[9,10]. In these studies, ^{65}Zn species from $ZnCl_2$ aqueous solution and ZnO suspension have been applied to the intact skin of rats or rabbits. ^{65}Zn species rapidly appear in the blood and other tissues. A total penetration of ^{65}Zn species from a carrier-free ^{65}Zn-$ZnCl_2$ solution at pH 1 and from a ^{65}Zn-ZnO suspension at pH 8 was detected. Autoradiography shows ^{65}Zn activity in both dermis and panniculus carnosus, mostly concentrated on or near the epidermis and around hair follicles in the dermis. Some reports maintain that ZnO and TiO_2 NPs, and even micronized TiO_2 in sunscreens, can pass through human skin too[11–14] although more systematic studies are necessary. It is important to note that only a minority of publications suggest the possibility of human dermal penetration and then only under certain conditions. On the other hand, there is a larger volume of work suggesting that NPs do not penetrate through healthy skin[3].

ZnO NPs are used as a sunscreen because it is a semiconductor with a bandgap of 3.3 eV, very close to the anatase gap energy of TiO_2[15]. Preliminary studies indicate that ZnO NPs (~15 nm) at concentrations of 3–10 mM cause 100% inhibition of *Escherichia coli*

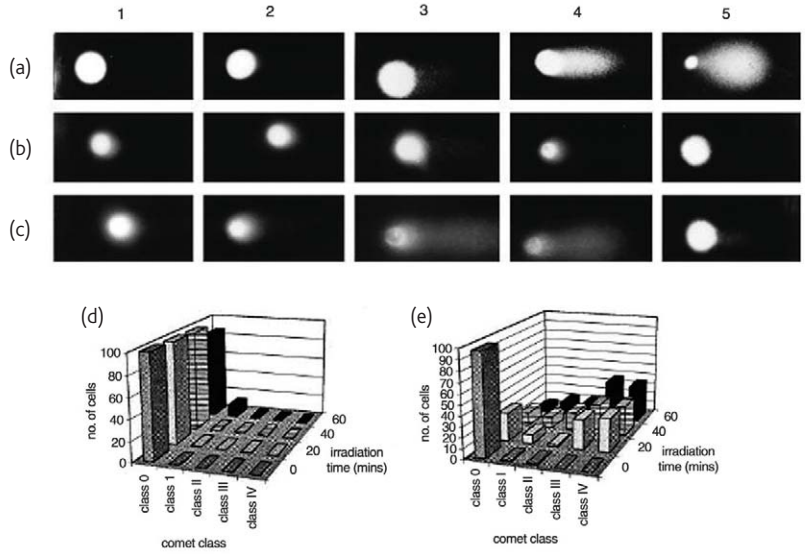

Fig. 2 Damage inflicted on human cells revealed by comet assays. Row (a): comets obtained using X-rays from a Gavitron RX30 source. The dose rate was 8.9 Gy min^{-1} and cells were exposed on ice for 0 s, 15 s, 30 s, and 60 s, giving comets falling into the five main standard classes shown: (1) class 0; (2) class I; (3) class II; (4) class III; and (5) class IV. Rows (b) and (c): examples of comets obtained using simulated sunlight, MRC-5 fibroblasts, and sunscreen TiO_2 (0.000125 % w/v). For each exposure, 100 cells were scored, and comets were classified by comparison with the standards, row (a). Row (b): no treatment (1); sunlight alone for 20 mins, 40 mins, and 60 mins (2–4); and effect of TiO_2 in the dark for 60 min (5). Row (c): sunlight with TiO_2 for 0 mins, 20 mins, 40 mins, and 60 mins (1–4); and for 60 min with TiO_2 and 200 mM DMSO (5). The charts summarize results from five independent experiments: (d) shows that sunlight alone inflicts few strand breaks and/or alkali-labile sites and (e) that inclusion of TiO_2 catalyses this damage. (Reproduced with permission from[8]. ©1997 Elsevier Ltd.)

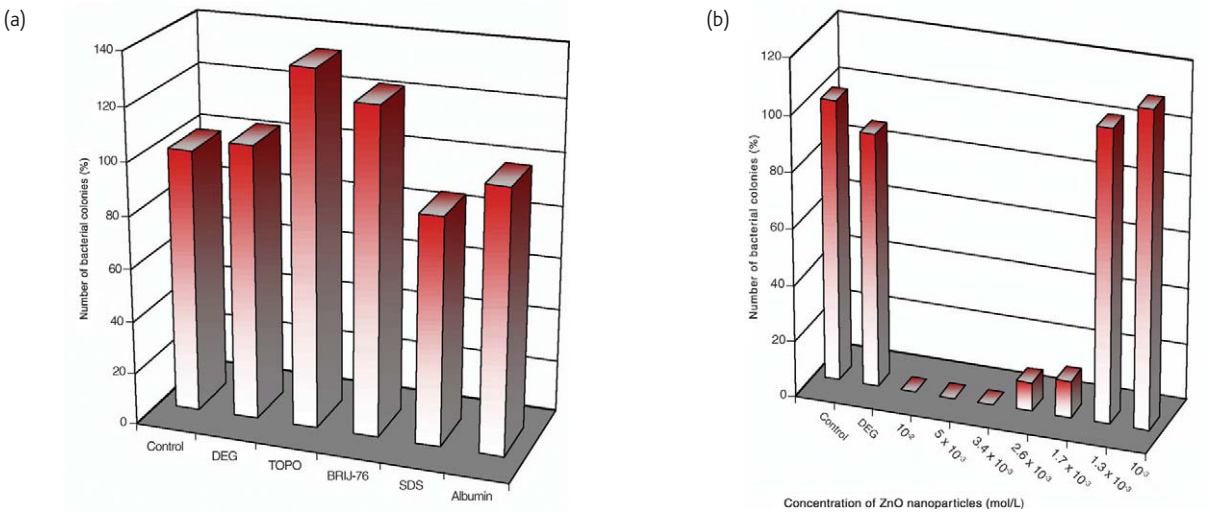

Fig. 3 Bactericidal tests as a function of (a) different small molecules and macromolecules and (b) ZnO concentration after incubation at 37°C overnight.

bacterial growth[15]. *E. coli* was used in this study because it is a model for antibacterial NPs. In this work, ZnO NPs were synthesized using the polyol process by forced hydrolysis of ionic Zn^{2+} salts in di(ethylene glycol) (DEG). Here, particle size and shape are controlled by the addition of small and macromolecules such as tri-*n*-octylphosphine oxide (TOPO), sodium dodecyl sulfate (SDS), polyoxyethylene stearyl ether (Brij-76), and bovine serum albumin (BSA). These molecules are often present in engineered nanomaterials because they are used to control size and shape during synthesis. Bacteriological tests (using *E. coli* strain MG1655) were performed on solid agar plates with different concentrations of small and macromolecules, as well as different concentrations of ZnO NPs. The inoculated cells were estimated to be 200 colony-forming units (CFU) per plate and all results were compared with a control without ZnO NPs. ZnO-free lysogeny broth (LB) agar plates and polyol-LB agar plates were used as a control[16]. It was observed that the number of bacterial colonies grown on the control, DEG, and albumin plates is quite similar (~100%) and growth is inhibited in the presence of SDS because of denaturalization of bacterial proteins (Fig. 3a). TOPO and Brij-76 molecules promote bacterial growth after they are metabolized (Fig. 3a). The same test was carried out with ZnO alone (without adsorbed molecules), varying the NP concentration from 10^{-2}–10^{-3} M. In this case, the lethal dose is observed between 10^{-2}–3.0 x 10^{-3} M (Fig. 3b). In addition, *E. coli* cells were damaged, showing a Gram-negative triple membrane disorganization and, consequently, ZnO internalization after contact with ZnO NP concentrations higher than 1.3 x 10^{-3} M and in the presence of some adsorbed molecules (Fig. 4). This bacterial damage may have a positive application. In fact, there is some evidence that ZnO NPs protect against intestinal diseases. However, despite the suggestion that ZnO may have an antibacterial effect, the mechanisms of this have not yet been elucidated.

Roselli *et al.*[17] have investigated the potential benefits of ZnO in protecting intestinal cells from damage induced by enterotoxigenic *E. coli* (ETEC, strain K88) and the related mechanisms, using human Caco-2 enterocytes. The integrity of the intestinal barrier is fundamental to the proper functioning of epithelial cells and to the prevention of the entry of pathogenic bacteria that cause inflammation[18]. Some report that Zn plays a role in maintaining epithelial barrier integrity and function. In fact, it has been shown that the treatment of porcine endothelial cells with Zn prevents tumor

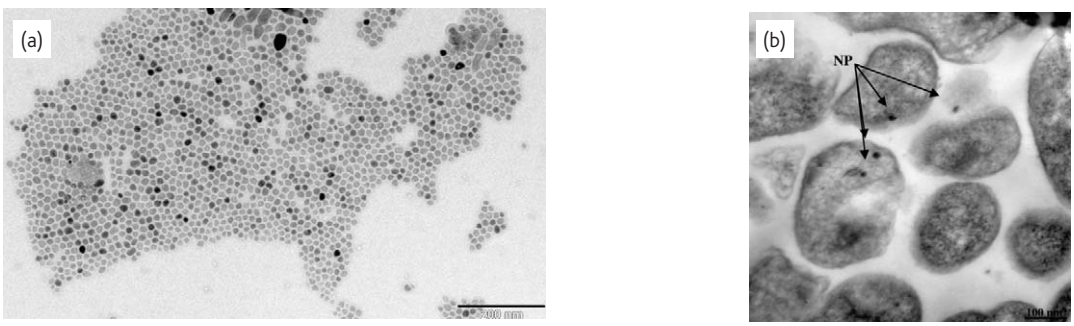

Fig. 4 (a) Transmission electron micrographs of (a) ZnO-TOPO NPs and (b) ZnO nanoparticle internalization by E. coli (thin sections).

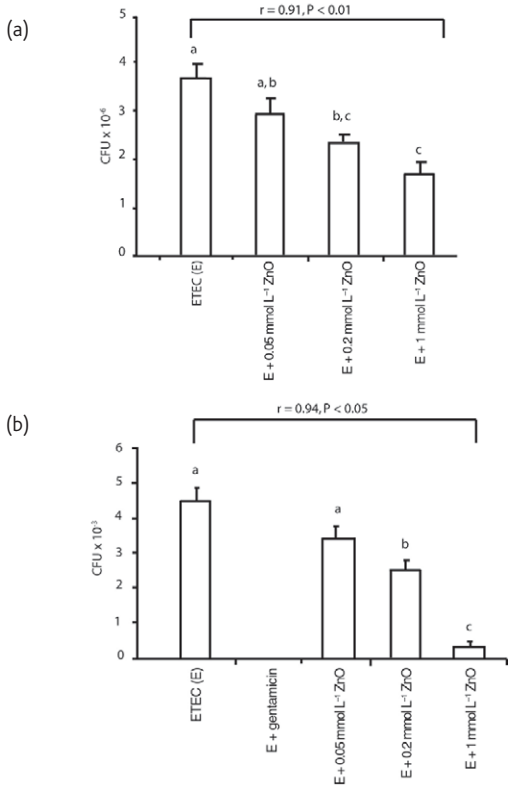

Fig 5 (a) Reduction of enterotoxigenic E. coli (ETEC) adhesion to Caco-2 cells by ZnO; (b) reduction of enterotoxigenic E. coli (ETEC) invasivity of Caco-2 cells by ZnO. (Reproduced with permission from[17]. ©2003 American Society for Nutrition.)

necrosis factor (TNF)-induced disruption of the cell monolayer and may also improve mucosal repair and paracellular permeability in experimental colitis[19–21]. Based on these results, Roselli *et al.*[17] show that a high percentage of ETEC adheres to Caco-2 cells 1.5 hrs after infection (Fig. 5a). Treatment with 0.2 mmol L^{-1} or 1 mmol L^{-1} ZnO NPs reduces bacterial adhesion, compared with infected cells. On the other hand, addition of only 0.05 mmol L^{-1} ZnO is ineffective. In addition, the ETEC invades Caco-2 cells after 2.5 hrs of challenge, although only small numbers of the total bacteria are internalized (Fig. 5b). In this case, treatment with ZnO induces a dose-dependent anti-invasive effect. The cytokine gene expression was also tested. Treatment with 0.2 mmol L^{-1} or 1 mmol L^{-1} of ZnO together with ETEC infection prevents alterations in cytokine expression induced by ETEC. In conclusion, ZnO NPs may protect intestinal cells from ETEC infection by inhibiting the adhesion and internalization of bacteria, preventing the increase of tight junction permeability and modulating cytokine gene expression.

Carbon-based nanomaterials

Carbon-based nanomaterials (CBNs) are important and exciting engineered nanomaterials that have stimulated a great deal of interest over the past decade. They have different forms such as fullerenes, single- and multiwalled CNTs (SWNTs and MWNTs, respectively), carbon NPs, and nanofibers. The scientific community is concerned about the toxicity of CNTs because of their structural resemblance to asbestos. Inhalation of asbestos fibers is known to induce asbestosis (a progressive fibrotic disease of the lung), lung cancer, and malignant mesothelioma of the pleura[22]. The mechanisms that lead from asbestos accumulation in the lung to disease are complex and experiments performed on rats or guinea pigs have been inconclusive (asbestos-induced disease takes longer than the lifetime of these animals to manifest itself)[23]. This carcinogenic silicate mineral has a fibrous form (like carbon nanofibers); consequently, the size, aspect ratio, and surface charge may have a strong influence on the toxicity[24]. However, it is important to note that asbestos has a micro- and not a nanofiber form, so we must take comparisons between asbestos and carbon nanofibers with caution.

From this point of view, Magrez *et al.*[25] have studied the cellular toxicity of CBNs (MWNTs, carbon nanofibers (CNFs), and carbon NPs) as a function of their aspect ratio and surface chemistry (Fig. 6). In this work, the effect of CBNs on cell proliferation and cytotoxicity was evaluated by the widely established 3-(4,5-dimethylthiazolyl-2)-2,5-diphenyltetrazolium bromide (MTT) assay[26] performed with three different human lung-tumor cell lines, H596, H446, and Calu-1. This assay is based on the accumulation of dark blue formazan crystals inside living cells after their exposure to MTT. The destruction of the cell membrane after the addition of DMSO results in the liberation and

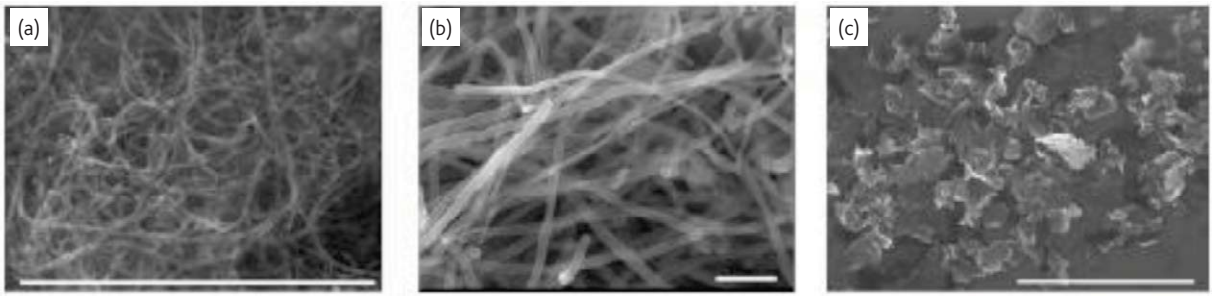

Fig. 6 Scanning electron micrographs of (a)MWNTs; (b) CNFs; and (c) carbon black. The aspect ratio of these NPs is about 80–90, 30–40 and 1, respectively. Scale bars: 2 μm. (Reproduced with permission from[25]. © 2006 American Chemical Society.)

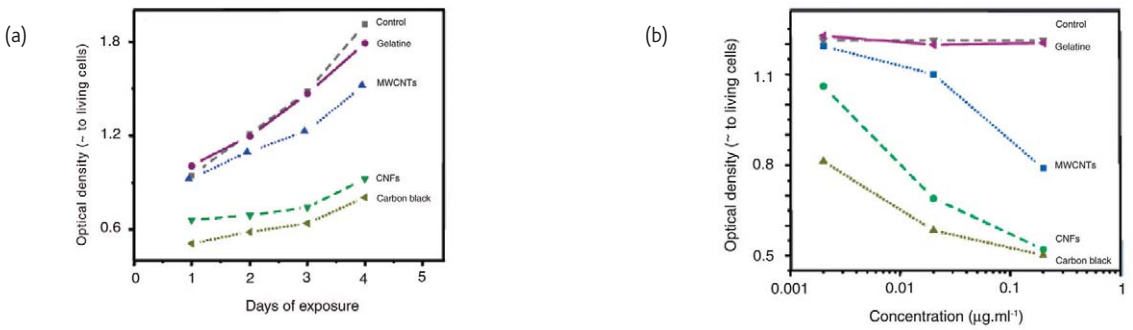

Fig. 7 (a) Representative growth curve for H596 cells grown in normal medium (control), medium containing gelatin, and 0.02 µg mL^{-1} of CBNs. MWNTs, CNFs, and carbon black are dispersed in the same gelatin-containing medium. (b) Dose-dependent toxicity of H596 cells exposed to CBNs for two days. (Reproduced with permission from[25]. © 2006 American Chemical Society.)

solubilization of the crystals. The number of viable cells is thus directly proportional to the level of the initial formazan product created. The formazan concentration is finally quantified using a spectrophotometer to measure the absorbance at 570 nm (enzyme-linked immunosorbent assay reader). For each cell type, a linear relationship between cell number and optical density is established, thus allowing an accurate quantification of changes in the rate of cell proliferation. Fig. 7a presents an average growth curve of H596 cells in a standard medium. The results show that the number of viable cells in all CBN-treated samples decreases. Analysis of the dose-dependent toxicity after two days of CBN exposure reveals that the number of viable cells decreases as a function of the CBN exposure dose for all CBNs tested (Fig. 7b). In all cases, the toxicity order is CB > CNFs > MWNTs. The authors also observed several morphological alterations of the cells exposed to different CBNs compared with the control cells, indicating a common final cell death pathway for all CBNs (Fig. 8).

Belyanskaya *et al.*[27] suggest a careful validation of MTT assay procedures is necessary in experiments where CNTs are one of the constituents. In their study, two MTT assays were applied to study the effect of single-walled CNTs (SWNTs) on the human epithelial cell line A549. Both assays reveal significant and comparable loss of cell functionality, confirmed by DNA assays. However, they also found that polyoxyethylene sorbitan monooleate-suspended SWNTs interfere less with MTT assay than sodium dodecyl sulfate-suspended SWNTs when using a cell-free system. Moreover, depending on the SWNTs purification procedure, the authors maintain that they are able to convert MTT into its MTT-formazan insoluble form in the absence of any living system.

To explore the effect of surface chemical properties on CBN toxicity, Dumortier *et al.*[28] have synthesized two types of functionalized carbon nanotubes (f-CNTs) following: (i) the 1,3-dipolar cycloaddition reaction (f-CNTs 1 and 2); and (ii) the oxidation/amidation treatment (f-CNTs 3 and 4) to study their impact on immune system cells (Fig. 9). They examined whether the different cell types present in the spleen and other lymphoid organs are susceptible to f-CNT penetration. They isolated B lymphocytes, T lymphocytes, and macrophages

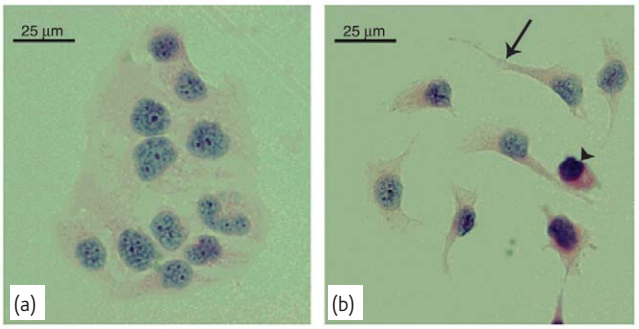

Fig. 8 Cytopathological analyses of H596 cells: (a) a typical control image of H596 cells where the cells are stained with hematoxyline-eosine, the nuclei appear purple and patchy, the cytoplasm is weekly stained (pink). Clusters of cells are characterized by close cell/cell contacts, and individual cells are polygon-shaped. (b) H596 cells after one day of treatment with 0.02 µg mL^{-1} MWNTs. Cells have lost their mutual attachments, retracted their cytoplasm (arrows) such that the pink color appears stronger, and the nuclei are smaller and more condensed (picnotic) also shown by the stronger purple staining. (Reproduced with permission from[25]. © 2006 American Chemical Society.)

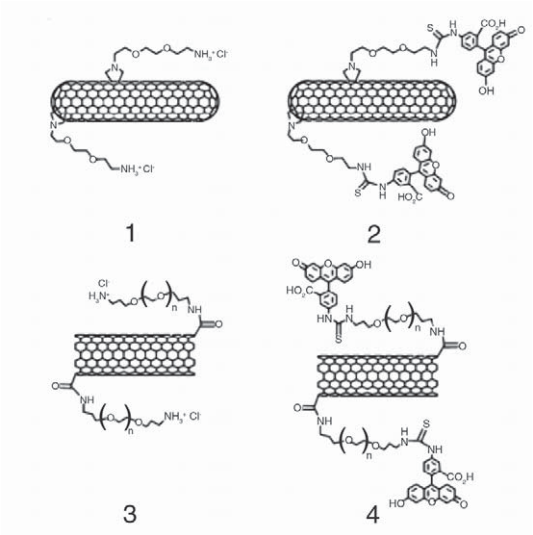

Fig. 9 Molecular structures of f-CNTs used in this study. (Reproduced with permission from[28]. © 2006 American Chemical Society.)

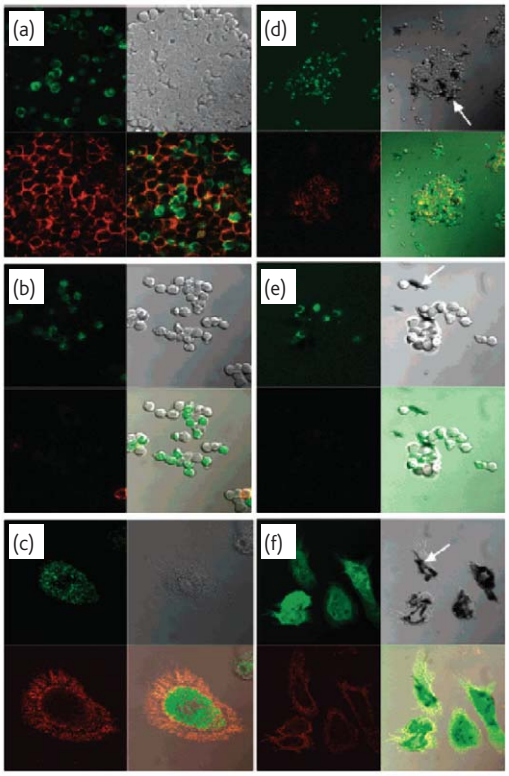

Fig. 10 f-CNTs localize inside B and T lymphocytes as well as macrophages. Three major immune cell populations, i.e. B lymphocytes (a, d), T lymphocytes (b, e), and macrophages (c, f), were isolated from the spleen, lymph nodes, and peritoneal cavity of BALB/c mice, respectively. They were incubated for 22–24 hrs with 10 μg mL^{-1} of either f-CNT 2 (a–c) and 4 (d–f). Plasma membrane staining (orange fluorescence) was then performed using antibodies specific either for MHC (major histocompatibility complex) class II molecules in the case of lymphocytes (expressed on B cells but not on T cells) and for the pan-marker F4-80 in the case of macrophages. The white arrows indicate bundles of f-CNT 4 that are located outside lymphocytes (d, e) but inside the cytoplasm of macrophages (f). Upper left quadrant, intracellular nanotubes (green fluorescence); upper right quadrant, visible light image; lower left quadrant, membrane staining (orange fluorescence); lower right quadrant, combined light and fluorescence images. (Reproduced with permission from[28]. © 2006 American Chemical Society.)

from the spleen, lymph nodes, and peritoneal cavity of BALB/c mice, respectively. The isolated cell populations were then incubated for 24 hrs with fluoresceine isothiocyanate (FITC)-labeled f-CNTS 2 and 4 at 10 μg mL^{-1}, washed, and stained with fluorescently labeled antibodies, specific for surface markers, before being examined by confocal microscopy (Fig. 10). The results show that both types of solubilized f-CNTs (visualized as green fluorescence) are found in the cytoplasm of the three cell types, suggesting that they have been actively captured by the cells or that they have diffused through the cell membrane. The images also show that not all cells are stained with fluorescent f-CNTs. Moreover, in the case of f-CNT 4, the authors found that these nanotubes form a suspension in water with the presence of some aggregates, which settle in the cell culture. Consequently, f-CNT 4 can be detected as big bundles in the medium around B and T lymphocytes (Figs. 10d, e) but not inside the macrophages (Fig. 10f). Following Dumortier *et al*., the latter observation supports the hypothesis that an active uptake mechanism is likely to be involved in the entry of f-CNTs into macrophages, widely know as highly phagocytic cells. Finally, the authors analyzed the impact of the two types of f-CNTs on primary immune cell viability to verify the existence of a direct correlation between the degree of functionalization of CNTs and the observed cytotoxic effects. For this purpose, purified B and T lymphocytes and macrophages were cultured in the presence of ammonium-functionalized CNT 1 and 3 and cell viability was assessed by flow cytometry after staining with two markers of cell death, corresponding to fluorescently labeled annexin V and propidium iodide (PI). No significant loss of cell viability was observed upon incubation of the three cell types with 10 μg mL^{-1} and 50 μg mL^{-1} of f-CNTs 1 and 3 for 24 hrs and 48 hrs, as compared with untreated cells indicating that f-CNTs do not induce primary immune cell death. This first important study of the impact of soluble f-CNTs on primary cells belonging to the immune system shows that these functionalized nanotubes do not induce cell death or activation of lymphocytes and macrophages, and they do not disturb cell functions. In conclusion, these results strengthen the promising possibility of using soluble f-CNTs as carriers of biological and therapeutic molecules without affecting the immune system.

Au nanoparticles

NPs are also currently receiving considerable attention because of their potential applications in biology and medicine but, in these cases, they must be water soluble and biocompatible. The increasing availability of nanostructures with highly controlled optical and magnetic properties in the nanometer size range has created widespread interest in their use in biotechnological systems for diagnostic applications and biological imaging[29,30]. Cellular imaging based on microscopy provides anatomic details of cells and tissue architecture important for cancer diagnostics and research. The optical probes currently used include chemiluminescent, fluorimetric, and colorimetric techniques[31]. Quantum dots such as CdS, CdSe, CdTe, and CdSe@ZnS are widely used and studied for these applications because of their unique size-dependent fluorescence properties, but their potential human toxicity and cytotoxicity are two major problems for *in vivo* applications[32,33]. Au NPs have become an alternative because of their simple preparation, ready bioconjugation, and potential noncytotoxicity[34]. Preliminary studies using surface plasmon resonance scattering and absorption have reported that anti-epidermal growth factor receptor (EGFR) antibody conjugated Au NPs specifically and homogeneously bind to the surface of cancer-type cells with 600% greater affinity than to noncancerous cells (Fig. 11)[35]. El-Sayed *et al*.[35] affirm that HaCaT noncancerous cells are poorly labeled by Au NPs (without conjugation with anti-EGFR antibodies) and that cells cannot be identified individually. When the conjugates are incubated with two malignant oral epithelial cell lines (HOC 313 clone 8 and HSC 3) for the same

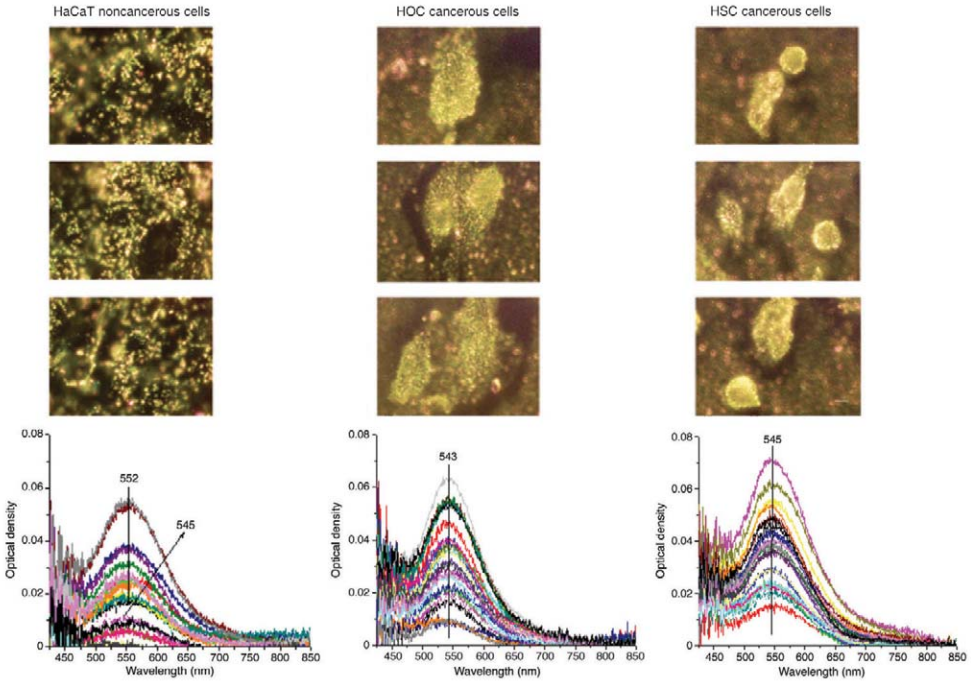

Fig. 11 Light scattering images and microabsorption spectra of HaCaT noncancerous cells (left column), human ovarian carcinoma (HOC) cancerous cells (middle column), and human squamous carcinoma (HSC) cancerous cells (right column) after incubation with anti-EGFR antibody conjugated Au NPs. Three different images of each kind of cells are shown to test reproducibility. The absorption spectra were measured for 25 different single cells. The figure shows clearly distinguishable differences in the scattering images from noncancerous cells (left column) and cancerous cells (right two columns). The conjugated NPs bind specifically with high concentrations to the surface of the cancer cells (right two columns). The conjugated NPs do not show aggregation tendencies (no long wavelength broad tail is observed). Scale bar: 10 μm for all images. (Reproduced with permission from[35]. © 2005 American Chemical Society.)

amount of time, the Au NPs are found on the surface of the cells, specially on the cytoplasm membranes for HSC cancer cells (Fig. 11).

This contrast difference is the result of specific binding of overexpressed EGFR on cancer cells with the anti-EGFR antibodies on the Au surface. It was also shown that a nonspecific interaction between the anti-EGFR antibodies and the collagen matrix also exists, which is shown as the reddish light scattering of the Au NPs on the collagen background (Fig. 11). In addition, when anti-EGFR antibodies are attached to Au NPs, all absorption spectra on different cells become narrower and similar for each cell type. No absorption bands arising from aggregation are observed. The NPs bonded to HOC and HSC cancer cells have similar absorption maxima at ~545 nm, which is 9 nm red shifted compared with isolated anti-EGFR/Au solutions at 536 nm. The authors confirm that this red shift is the result of specific binding of anti-EGFR antibodies on the Au surface to EGFR on the cell surface. These results suggest that surface plasmon resonance (SPR) scattering imaging or SPR absorption spectroscopy generated from antibody conjugated Au NPs can be useful in molecular biosensor techniques for the diagnosis and investigation of oral epithelial living cancer cells *in vivo* and *in vitro*.

Recent literature, however, contains conflicting data regarding the cytotoxicity of Au NPs[36–38]. Against this background, a systematic study of water-soluble Au NPs stabilized by triphenylphosphine derivatives ranging in size from 0.8–15 nm has been performed by Pan *et al.*[38]. In this study, the authors worked with HeLa cervix carcinoma epithelial cells (HeLa), SK-Mel-28 melanoma cells (SK-Mel-28), L929 mouse fibroblasts (L929), and mouse monocytic/macrophage cells (J774A1). The toxicity of Au compounds was quantified by determining the IC_{50} values (the half maximal inhibitory concentration – the concentration of an inhibitor that is required to achieve 50% target inhibition) in MTT assays. The authors performed these tests during both logarithmic and stationary phases of cell growth. Invariably, cells during the logarithmic growth phases are 1.5–3.3-fold more sensitive to toxic Au compounds than during the stationary phase. In contrast, Au NPs 15 nm in size are nontoxic at up to 60-fold concentration. Transmission electron microscopy (TEM) studies show that the cellular response is size dependent – 1.4 nm NPs cause rapid cell death by necrosis within 12 hrs while the closely related 1.2 nm NPs result in programmed cell death by apoptosis.

Cytotoxicity of inhaled nanoparticles

Recent epidemiological studies provide evidence that an increase in atmospheric NPs is associated with adverse cardiovascular effects in susceptible individuals such as the elderly and those suffering from underlying diseases of various origins[39,40]. Lung retention and clearance of inhaled NPs <100 nm in diameter by alveolar macrophages is

thought to be less effective than for larger particles. This is because macrophages *in vivo* are not as efficient at phagocytizing NPs >100 nm[41] as they are at phagocytizing particles. A common approach to investigating the clearance kinetics of NPs in lungs is the use of poorly soluble particles labeled with a convenient radioactive γ emitter. Semmler-Behnke *et al.*[42] have found ^{192}Ir to be an appropriate material for studying clearance kinetics because of its very low solubility, even in the NP domain. They have studied the disappearance of ^{192}Ir NPs from the epithelium by taking sequential lung retention, clearance, and bronchoalveolar lavage measurements in healthy adult Wistar Kyoto rats at various times over six months following intratracheal inhalation of a single 60–100 min dose of ^{192}Ir NPs. The authors conclude that there is a strong size-selective difference in NP immobilization. NPs are less easily phagocytized by alveolar macrophages than larger particles but they are effectively removed from the lung surface into the interstitium. Even from these interstitial sites, they undergo alveolar macrophage-mediated long-term NP clearance to the larynx.

Several studies have shown that inhaled CB particles induce lung tumors in rats but not in other rodent species[43] when administered at doses that cause particle overload in the lungs, as well as chronic inflammation and epithelial hyperplasia. CB is not directly mutagenic, therefore, tumor formation in rats must occur via a secondary mechanism. Elder *et al.*[44] have studied particle retention kinetics, inflammation, and histopathology in female rats, mice, and hamsters exposed for 13 weeks to high surface area CB at doses chosen to span a *no observed adverse effects level* (NOAEL) to particle overload (0 mg m^{-3}, 1 mg m^{-3}, 7 mg m^{-3}, 50 mg m^{-3}, nominal concentrations). Retention and effects measurements were performed immediately after exposure and three and eleven months post exposure. Significant decreases in body weight during exposure only occur in hamsters exposed to high-dose HSCB. Lung weights increase in high-dose CB-exposed animals, but this persists only in rats and mice. The authors conclude that a subchronic NOAEL of 1 mg m^{-3} respirable HSCB can be assigned to female rats, mice, and hamsters.

Conclusions

We can draw the following conclusions regarding the examples cited. NPs may enter the human body via the lungs and the intestines (if ingested); penetration via the skin is less evident but it is possible that some NPs can penetrate deep into the dermis. NP internalization depends on the particle size, surface properties, and functionalization. After internalization, the NP distribution in the body is a strong function of the NP's surface characteristics. In addition, the presence of contaminants, such as metal catalysts used to synthesize CNTs (not shown in this review), and their role in observed health effects should be also examined. nt

Acknowledgments

ZnO NP toxicological studies were supported by ANR-05-ECCO-001-08 (France).

References

1. Erhardt, D., *Nat. Mater.* (2003) **2**, 509
2. www.mpikg-golm.mpg.de
3. Kumar, C., (ed.) *Nanomaterials – Toxicity, Health and Environmental Issues, Nanotechnologies for the Life Sciences*, Wiley-VCH, (2006), 5
4. Maynard, R. L., and Howard, C. V., (eds.), *Particulate Matter: Properties and Effects Upon Health,* Oxford, BIOS Scientific Publishers in association with the Royal Microscopical Society, (1999), 115
5. Donaldson, K., *et al.*, *Occup. Environ. Med.* (2001) **58**, 211
6. Donaldson, K., *et al.*, *Philos. Trans. R. Soc. London, Ser. A* (2000) **358**, 2741
7. Wilson, M. R., *et al.*, *Toxicol. Appl. Pharmacol.* (2002) **184**, 172
8. Dunford, R., *et al.*, *FEBS Lett.* (1997) **418**, 87
9. Hallmans, G., and Liden, S., *Acta Dermatol. Venereol.* (1979) **59**, 105
10. Kapur, S. P., *et al.*, *Proc. Soc. Exp. Biol. Med.* (1974) **145**, 932
11. Agren, M. S., *Dermatologica* (1990) **180**, 36
12. Dupre, A., *et al.*, *Arch. Dermatol.* (1985) **121**, 656
13. Moran, C. A., *et al.*, *Human Pathol.* (1991) **22**, 450
14. Tan, M. H., *et al.*, *J. Dermatol.* (1996) **37**, 185
15. Strehlow, W. H., and Cook, E. L., *J. Phys. Chem. Ref. Data* (1973) **2**, 163
16. Brayner, R., *et al.*, *Nano Lett.* (2006) **6**, 866
17. Roselli, M., *et al.*, *J. Nutr.* (2003) **133**, 4077
18. Lu, L., and Walker, W. A., *Am. J. Clin. Nutr.* (2001) **73**, 1124S
19. Hennig, B., *et al. J. Nutr.* (1992) **122**, 1242
20. Hennig, B., *et al. J. Nutr.* (1993) **123**, 1003
21. Sturniolo, G. C., and Fries, W., *J. Lab. Clin. Med.* (2002) **139**, 311
22. LaDou, J., *Environ. Health Perspect.* (2004) **112**, 285
23. Huczko, A., *et al.*, *Fullerenes, Nanotubes, Carbon Nanostruct.* (2001) **9**, 251
24. Rogers, R. A., *et al.*, J. M., *Environ. Health Perspect.* (1999) **107**, 367
25. Magrez, A., *et al.*, *Nano Lett.* (2006) **6**, 1121
26. Mosmann, T., *J. Immunol. Methods* (1983) **65**, 55
27. Belyanskaya, L., *et al.*, *Carbon* (2007) **45**, 2643
28. Dumortier, H., *et al.*, *Nano Lett.* (2006) **12**, 3003
29. Alivisatos, A. P., *Nat. Biotech.* (2004) **22**, 47
30. Wickline, S. A., and Lanza, G. M., *Circulation* (2003) **107**, 1092
31. Roda, A., *et al.*, *Bioluminescence and Chemiluminescence: Perspectives for the 21st Century*, Wiley, Chichester (1999)
32. Bruchez, M. Jr., *et al.*, *Science* (1998) **281**, 2013
33. Chan, W. C. W., and Nie, S., *Science* (1998) **281**, 2016
34. West, J. L., and Halas, N. J., *Curr. Opin. Biotech.* (2002) **11**, 215
35. El-Sayed, I. H., *et al. Nano Lett.* (2005) **5**, 829
36. Tsoli, M., *et al.*, *Small* (2005) **1**, 841
37. Pernodet, N., *et al.*, *Small* (2006) **2**, 766
38. Pan, Y., *et al.*, *Small* (2007) **3**, 1941
39. Ibald-Mulli, A., *et al.*, *J. Aerosol Med.* (2002) **15**, 189
40. Wichmann, H. E., and Peters, A., *Philos. Trans. R. Soc. London, Ser. A* (2000) **358**, 2751
41. Kreyling, W. G., and Scheuch, G., Clearance of Particles Deposited in the Lungs in *Particle-lung interactions* (2000), New York/Basel, Marcel Dekker, 323
42. Semmler-Behnke, M., *et al.*, *Environ. Health Perspect.* (2007) **115**, 728
43. Rausch, L. J., *et al.*, *Reg. Toxicol. Pharmacol.* (2004) **40**, 28
44. Elder, A., *et al.*, *Toxicol. Sci.* (2005), **88**, 614